Acta Crystallographica Section D
**Biological Crystallography**
ISSN 0907-4449

# Structures of enzyme–intermediate complexes of yeast Nit2: insights into its catalytic mechanism and different substrate specificity compared with mammalian Nit2

**Hejun Liu,[a,b] Yongxiang Gao,[a,b] Mengying Zhang,[a,b] Xiaoting Qiu,[a,b] Arthur J. L. Cooper,[c] Liwen Niu[a,b]* and Maikun Teng[a,b]***

[a]Hefei National Laboratory for Physical Sciences at the Microscale and School of Life Science, University of Science and Technology of China, Hefei, Anhui 230026, People's Republic of China, [b]Key Laboratory of Structural Biology, Chinese Academy of Sciences, Hefei, Anhui 230026, People's Republic of China, and [c]Department of Biochemistry and Molecular Biology, New York Medical College, Valhalla, NY 10595, USA

Correspondence e-mail: lwniu@ustc.edu.cn, mkteng@ustc.edu.cn

Received 27 February 2013
Accepted 6 April 2013

**PDB References:** yNit2, wild type, 4h5u; complex with α-ketoglutarate, 4hg3; complex with oxaloacetate, 4hg5; C169S mutant, 4hgd

The Nit (nitrilase-like) protein subfamily constitutes branch 10 of the nitrilase superfamily. Nit proteins are widely distributed in nature. Mammals possess two members of the Nit subfamily, namely Nit1 and Nit2. Based on sequence similarity, yeast Nit2 (yNit2) is a homologue of mouse Nit1, a tumour-suppressor protein whose substrate specificity is not yet known. Previous studies have shown that mammalian Nit2 (also a putative tumour suppressor) is identical to ω-amidase, an enzyme that catalyzes the hydrolysis of α-ketoglutaramate (α-KGM) and α-ketosuccinamate (α-KSM) to α-ketoglutarate (α-KG) and oxaloacetate (OA), respectively. In the present study, crystal structures of wild-type (WT) yNit2 and of WT yNit2 in complex with α-KG and with OA were determined. In addition, the crystal structure of the C169S mutant of yNit2 (yNit2-C169S) in complex with an endogenous molecule of unknown structure was also solved. Analysis of the structures revealed that α-KG and OA are covalently bound to Cys169 by the formation of a thioester bond between the sulfhydryl group of the cysteine residue and the γ-carboxyl group of α-KG or the β-carboxyl group of OA, reflecting the presumed reaction intermediates. However, an enzymatic assay suggests that α-KGM is a relatively poor substrate of yNit2. Finally, a ligand was found in the active site of yNit2-C169S that may be a natural substrate of yNit2 or an endogenous regulator of enzyme activity. These crystallographic analyses provide information on the mode of substrate/ligand binding at the active site of yNit2 and insights into the catalytic mechanism. These findings suggest that yNit2 may have broad biological roles in yeast, especially in regard to nitrogen homeostasis, and provide a framework for the elucidation of the substrate specificity and biological role of mammalian Nit1.

## 1. Introduction

Enzymes of the nitrilase superfamily are widely distributed in plants, animals, fungi and prokaryotes (Pace & Brenner, 2001). All enzymes in the nitrilase superfamily contain an active-site cysteine (O'Reilly & Turner, 2003; Howden & Preston, 2009). Based on sequence similarity and domain-fusion patterns, the nitrilase superfamily has been classified into 13 branches, nine of which have known or predicted nitrilase (only found in branch 1), amidase or amidotransferase activities (Pace & Brenner, 2001; Huebner *et al.*, 2011). Branch 10 contains two proteins, namely Nit1 and Nit2, both of which were predicted to have amidase activity at the time that the classification was published (Pace & Brenner, 2001). Nit1 and Nit2 are present in mammals, yeast and many other organisms. In fruit flies and nematodes Nit1 is present as a NitFhit fusion protein, whereas in mammals Nit1 and Fhit (fragile histidine triad) are discrete proteins (Pace & Brenner, 2001). Since the first identification

of nitrilase activity in plants in 1958 and in bacteria in 1964, over 30 true nitrilases have been documented and studied (Howden & Preston, 2009). As a group, nitrilases are perhaps the most well studied of the enzymes in the nitrilase superfamily. Here, we are concerned with branch 10 of the nitrilase superfamily, especially with the possible role of Nit2 in nitrogen homeostasis in yeast. There is considerable evidence to suggest that Nit1 is a potent tumour suppressor in mammals by stimulating apoptosis in cancer cells (Semba *et al.*, 2006; Sun *et al.*, 2009; Zhang *et al.*, 2009; Huebner *et al.*, 2011; Sun *et al.*, 2011). Fhit is also a tumour suppressor (Saldivar *et al.*, 2013), and the tumour-suppressor activities of Nit1 and Fhit may be additive (Sun *et al.*, 2009). However, the metabolic role and substrate specificity of mammalian Nit1 are unknown. Thus, it is not yet clear whether the Nit1 and Fhit enzymes are involved in a common metabolic pathway. Interestingly, there is now evidence to suggest that Nit2 is also a tumour suppressor. In this case, however, overexpression of Nit2 in HeLa cells leads to a decrease in cell growth and proliferation that is induced by G2 arrest rather than by apoptosis (Lin *et al.*, 2007).

Mammalian Nit2 has recently been identified as $\omega$-amidase (EC 3.5.1.3; Jaisson *et al.*, 2009; Krasnikov, Chien *et al.*, 2009; Krasnikov, Nostramo *et al.*, 2009; Chien *et al.*, 2012), an enzyme that was first discovered more than 55 years ago by Meister and coworkers (Meister *et al.*, 1952, 1955; Meister, 1953, 1954; Otani & Meister, 1957). $\omega$-Amidase purified from rat liver hydrolyzes $\alpha$-ketoglutaramate ($\alpha$-KGM) and $\alpha$-ketosuccinamate ($\alpha$-KSM), the $\alpha$-keto-acid analogues of glutamine and asparagine, respectively, to $\alpha$-ketoglutarate ($\alpha$-KG) and oxaloacetate (OA), respectively, with high efficiency (Meister *et al.*, 1955; Otani & Meister, 1957; Hersh, 1971, 1972). Glutamine and asparagine are not substrates of the rat enzyme (Meister, 1954; Meister *et al.*, 1955). In more recent studies, recombinant human Nit2 (hNit2; Krasnikov, Chien *et al.*, 2009; Chien *et al.*, 2012) and mouse Nit2 (mNit2) (Jaisson *et al.*, 2009) have also been shown to have high activity towards $\alpha$-KGM. Interestingly, rat liver $\omega$-amidase also efficiently catalyzes the hydrolysis of a variety of $\gamma$-esters of $\alpha$-ketoglutarate (Hersh, 1971, 1972). Recent studies have shown that mNit2/$\omega$-amidase has exceptionally high esterase activity toward the mono $\gamma$-methyl ester of $\alpha$-ketoglutarate (Jaisson *et al.*, 2009). Although mammalian Nit2 shares more than 40% sequence identity with mammalian Nit1 (Barglow *et al.*, 2008), it has been reported that mouse Nit1 (mNit1) exhibits no detectable activity towards $\alpha$-KGM (Jaisson *et al.*, 2009). However, in a personal communication two of the authors (S. Jaisson and E. Van Schaftingen) of this report indicated that mNit1 exhibits a specific activity of about 0.1% relative to that exhibited by mNit2 with $\alpha$-KGM as a substrate. Barglow *et al.* (2008) have investigated the active-site topologies of Nit1 and Nit2 by using various rhodamine-tagged dipeptides containing an $\alpha$-chloroacetamide moiety (dipeptide-$\alpha$-CA) as a probe to covalently label the catalytic cysteine (Barglow & Cravatt, 2006; Barglow *et al.*, 2008). This strategy was also used to investigate the active site of another member of the nitrilase superfamily, mouse $\beta$-ureidopropionase (Up$\beta$), an enzyme that has considerable sequence homology to mNit1 and mNit2 (Barglow & Cravatt, 2006). The active-site cysteine residues of mNit1, mNit2 and mouse Up$\beta$ exhibited different abilities to react with the various dipeptide probes, presumably reflecting different topologies of their respective active sites.

Despite advances in our understanding of the reactions catalyzed by Up$\beta$ and mammalian Nit2/$\omega$-amidase, the substrate specificity of mammalian Nit1 remains unknown. We reasoned that in order to fully understand the biological importance of the Nit family it is necessary to expand our knowledge of these enzymes to include non-mammalian Nit proteins. To this end, we have initiated a detailed investigation of the catalytic and structural properties of yeast Nit2 (yNit2). Since yNit2 shows considerable sequence homology to mammalian Nit1, such studies will not only advance our knowledge of the role of Nit protein(s) in nitrogen homeostasis in yeast but will also suggest a possible substrate for mammalian Nit1. We have now determined the crystal structures of yNit2 (i) crystallized in the absence of ligands, (ii) crystallized with covalently bound $\alpha$-KG in the active site and (iii) crystallized with OA covalently bound in the active site. In addition, we have also determined the crystal structure of a C169S mutant of yNit2 (yNit2-C169S) with an uncharacterized glutathione-like ligand in the active site. This finding suggests that Nit proteins may have even wider substrate specificity than previously recognized and/or that the activity is regulated by endogenous ligands.

## 2. Experimental procedures

### 2.1. Expression and purification of Nit2

The open reading frame of yNit2 was amplified by PCR using *Saccharomyces cerevisiae* S288c genomic DNA as the template and cloned into pET28a (Novagen) vector. The open reading frame of hNit2 was amplified from a human brain cDNA library and cloned into pET28a vector for protein expression. The correctness of the constructs was confirmed by sequencing. The recombinant yNit2 and hNit2 proteins containing a terminal hexahistidine ($His_6$) tag were expressed in *Escherichia coli* BL21(DE3) cells (Stratagene) and purified on a nickel column as outlined below.

The wild-type (WT) yNit2 expression construct was transformed into bacterial cells and 2 l of this construct in Luria–Bertani medium was inoculated with 50 $\mu$g ml$^{-1}$ kanamycin. After overnight incubation at 310 K with gentle shaking (220 rev min$^{-1}$) the $OD_{600}$ reached 0.8. At this point, Nit2 overexpression was induced with 0.25 m*M* isopropyl $\beta$-D-1-thiogalactopyranoside. After cooling the suspension to 303 K and incubation for a further 8 h, the *E. coli* cells were harvested by centrifugation at 5000*g* for 8 min at 281 K, resuspended in lysis buffer (50 m*M* Tris–HCl pH 8.0, 500 m*M* NaCl) and sonicated on ice for 20 min. The resulting supernatant solution, after removal of cell debris by centrifugation, was loaded onto a Ni–NTA column (Tiangen Biotech) equilibrated with lysis buffer. The target protein ($His_6$-tagged

**Table 1**
Crystallographic data-collection and structure-determination statistics.

Values in parentheses are for the outermost resolution shell.

| | WT yNit2 | yNit2–α-KG | yNit2–OA | yNit2-C169S |
|---|---|---|---|---|
| Data collection | | | | |
| Space group | $P2_1$ | $P2_1$ | $P2_1$ | $P2_1$ |
| Unit-cell parameters (Å, °) | $a$ = 65.3, $b$ = 125.7, $c$ = 77.7, $\alpha = \gamma$ = 90.0, $\beta$ = 95.2 | $a$ = 65.2, $b$ = 125.7, $c$ = 78.0, $\alpha = \gamma$ = 90.0, $\beta$ = 95.3 | $a$ = 65.5, $b$ = 125.8, $c$ = 77.9, $\alpha = \gamma$ = 90.0, $\beta$ = 95.5 | $a$ = 65.6, $b$ = 126.9, $c$ = 77.6, $\alpha = \gamma$ = 90.0, $\beta$ = 95.6 |
| Resolution range (Å) | 50.00–1.92 (1.94–1.92) | 50.00–1.93 (1.98–1.93) | 50.00–1.91 (1.94–1.91) | 50.00–2.03 (2.07–2.03) |
| Unique reflections | 95100 (4714) | 92806 (4616) | 92892 (4690) | 76148 (2679) |
| Completeness (%) | 100.0 (100.0) | 99.8 (99.9) | 95.8 (97.1) | 95.1 (93.2) |
| Average multiplicity | 3.8 (3.7) | 3.3 (3.3) | 2.5 (2.2) | 2.1 (2.0) |
| Mean $I/\sigma(I)$ | 23.18 (4.81) | 6.03 (2.12) | 7.44 (2.58) | 8.96 (2.38) |
| $R_{\rm merge}$† (%) | 9.5 (34.8) | 17.4 (61.0) | 9.5 (38.4) | 7.9 (59.5) |
| Refinement statistics | | | | |
| $R$ factor‡ (%) | 17.2 | 18.7 | 20.0 | 19.0 |
| $R_{\rm free}$§ (%) | 20.1 | 22.5 | 22.9 | 22.8 |
| R.m.s.d.,¶ bond lengths (Å) | 0.0131 | 0.0077 | 0.0071 | 0.0077 |
| R.m.s.d., bond angles (°) | 1.1597 | 1.1005 | 1.0630 | 1.0740 |
| Mean $B$ factors (Å$^2$) | | | | |
| Main chain | 14.7 | 13.3 | 27.3 | 22.1 |
| Side chain | 17.3 | 15.7 | 28.6 | 23.1 |
| Ramachandran plot†† (% of residues) | | | | |
| Favoured | 98.4 | 98.2 | 98.0 | 97.2 |
| Allowed | 1.6 | 1.8 | 2.0 | 2.5 |
| Outliers | 0 | 0 | 0 | 0.3 [Ser169, chain *A*/*B*/*C*/*D*] |
| PDB code | 4h5u | 4hg3 | 4hg5 | 4hgd |

† $R_{\rm merge} = \sum_{hkl}\sum_i |I_i(hkl) - \langle I(hkl)\rangle| / \sum_{hkl}\sum_i I_i(hkl)$, where $I_i(hkl)$ is the intensity of the $i$th observation and $\langle I(hkl)\rangle$ is the mean value for reflection $hkl$. ‡ $R$ factor = $\sum_{hkl} ||F_{\rm obs}| - |F_{\rm calc}|| / \sum_{hkl} |F_{\rm obs}|$, where $F_{\rm obs}$ and $F_{\rm calc}$ are the observed and calculated structure-factor amplitudes, respectively. § $R_{\rm free}$ is equivalent to the $R$ factor, but calculated with reflections excluded from the refinement process (5% of all reflections). ¶ Root-mean-square deviation from ideal values. †† The categories were defined by *MolProbity*.

yNit2, hereafter simply referred to as yNit2 or WT yNit2) was eluted by means of an imidazole gradient and further purified by gel filtration using a Superdex 200 column (GE Healthcare) pre-equilibrated with lysis buffer. Fractions containing pure protein, as indicated by SDS–PAGE, were pooled and concentrated using a centrifugal filter (Amicon). For crystallization experiments, the buffer was changed to 20 m*M* MES pH 6.5, 50 m*M* NaCl and the yNit2 was diluted to 20 mg ml$^{-1}$ in this buffer. SDS–PAGE analysis revealed a single band with the expected molecular weight of the yNit2 monomer with a $His_6$ tag (38 235). yNit2 mutants and hNit2 proteins were expressed and purified in the same manner as used for the WT protein and also resulted in a single band on SDS–PAGE.

### 2.2. Crystallization and data collection of WT yNit2, yNit2–α-KG, yNit2–OA and yNit2-C169S

Crystals of WT yNit2 were initially obtained by mixing 0.15 µl protein solution (20 mg ml$^{-1}$) with an equal volume of reservoir solution using a Mosquito crystallization robot (TTP LabTech). Optimal WT yNit2 crystals used for diffraction were produced manually by mixing 1 µl protein solution with 1 µl reservoir solution (17.5% PEG 4000, 0.1 *M* sodium cacodylate pH 6.5) followed by equilibration of this mixture against 100 µl mother liquor by the hanging-drop vapour-diffusion procedure over a period of about 10 d. Crystals of yNit2 containing α-KG (or OA) covalently bound at the active site (designated yNit–α-KG and yNit2–OA, respectively) were obtained by the procedure described above except that prior to the crystallization step the yNit2 protein (20 mg ml$^{-1}$) was incubated on ice with 25 m*M* α-KG sodium salt (Sigma) or 100 m*M* OA (Sigma) for 1 h. Both α-keto-acid solutions were titrated to pH 7.0 with 1 *M* NaOH. Crystals of the yNit2-C169S mutant were obtained under similar crystallization conditions with only minor pH optimization. All crystals employed for data diffraction were crystallized at 288 K and flash-cooled with liquid nitrogen after a short immersion in a cryoprotectant buffer consisting of 25%(*v*/*v*) glycerol in the reservoir solution. All diffraction data were collected in a stream of nitrogen gas at 100 K. Diffraction data for WT yNit2 were collected on beamline 17U at Shanghai Synchrotron Radiation Facility (SSRF) at a wavelength of 0.97792 Å using an MX-225 CCD detector (Rayonix LLC). Diffraction data for yNit2–α-KG, yNit2–OA and yNit2-C169S were collected on beamline 17U at SSRF at wavelengths of 0.97907, 0.97917 and 0.97930 Å, respectively, using a Quantum 315r detector (Area Detector Systems Corporation). All image data were processed, integrated and scaled in the monoclinic lattice $P2$ using the *HKL*-2000 software package (Otwinowski & Minor, 1997). Systematic absences indicated the space group to be $P2_1$.

### 2.3. Structure determination and refinement

Initial phases for the structure of WT yNit2 were obtained by the molecular-replacement method using *Phaser* (McCoy *et al.*, 2007) with yNit2 aligned with the Nit portion of the *Caenorhabditis elegans* NitFhit (cNitFhit) fusion-protein model (PDB entry 1ems; Pace *et al.*, 2000) as the query model and reflection data in the resolution range 48.8–2.5 Å. The structure of the Nit portion was used as the query model because based on sequence similarity the active site of yNit2

should be more like that of the Nit portion of cNitFhit than that of mammalian Nit2. The structures of the yNit2–α-KG, yNit2–OA and yNit2-C169S structures were determined by molecular replacement with *MOLREP* (Vagin & Teplyakov, 2010) using one of the monomers in the asymmetric unit of the finally refined WT yNit2 structure (*i.e.* WT yNit2 containing no bound ligand in the active site) as the search model. Model refinements were carried out by alternating rounds of manual building in *Coot* (Emsley *et al.*, 2010) and restrained refinement in *REFMAC*5 (Murshudov *et al.*, 2011) from the *CCP*4 suite of programs (Winn *et al.*, 2011). TLS parameters were included during the final refinement step of the yNit2-C169S mutant structure. For yNit2 crystallized in the presence of ligands, structural restraints for these ligands were generated by the *eLBOW* (Moriarty *et al.*, 2009) module of the *PHENIX* software (Adams *et al.*, 2010) given the simplified molecular-input line-entry specifications (SMILES) of the corresponding ligand covalently bonded to cysteine or *N*-(4-carboxy-4-oxobutanoyl)-L-cysteinylglycine (KGT; the putative structure of the ligand bound noncovalently to the active site of the yNit2-C169S mutant; see §3). The final refined models of WT yNit2, WT yNit2 with covalently bound ligands and the yNit2-C169S mutant with noncovalently bound ligand were completed in *Coot* with reasonable values of the *R* factor and free *R* factor. The overall assessment of model quality was validated with the *MolProbity* server (Chen *et al.*, 2010). Data-collection statistics, model refinement and the stereochemical quality of these structures are summarized in Table 1.

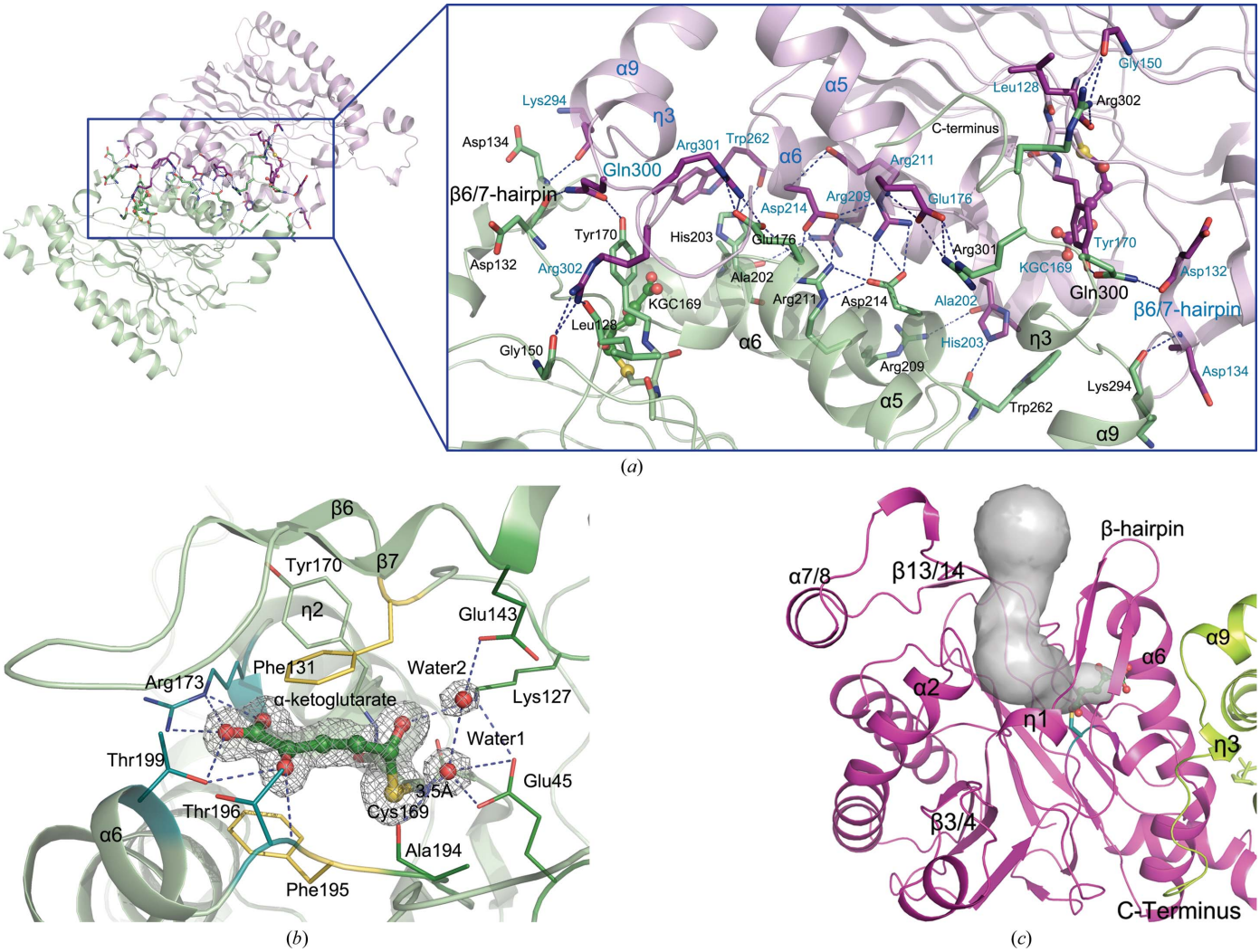


**Figure 1**
Dimerization of yNit2 subunits and covalent binding of α-KG near the dimer interface. Dashed lines represent hydrogen bonds and salt bridges. (*a*) Dimer interface of the yNit2–α-KG dimer. Monomers are shown in light green and light purple, respectively. Atoms in residues involved in the interface interactions are highlighted with conventional colours (*i.e.* O, red; N, blue; S, yellow). Gln300 mediates an interaction between the hairpin lid and the catalytic site. KGC169 represents α-KG covalently bound as a thioester to Cys169 and is depicted in ball-and-stick representation. (*b*) Ligand-site representation of yNit2–α-KG. The ligand linked by a thioester to Cys169 is buried in a deep cavity below the β6/7-hairpin. A $2F_o - F_c$ electron-density map at $1.2\sigma$ is constructed around the ligand at a radius of 1.6 Å. Arg173, Thr199 and Thr196 recognize the ligand functional groups, whereas Phe131 and Phe195 pack the ligand between them to form a sandwich-like configuration. Water1 (confined by the α-carboxyl of Glu45, the peptide-bond O atom of Ala194 and water2, which is in turn confined by Glu143) is 3.5 Å from the S atom of the α-KG thioester intermediate. The ε-amino group of Lys127 hydrogen bonds to the carbonyl group of this thioester. (*c*) *CAVER* analysis of yNit2. α-KG was selected as a starting point for the *CAVER* calculation. The solid grey surface represents the cavity. Each monomer in the dimer is represented in a different colour (red and green).

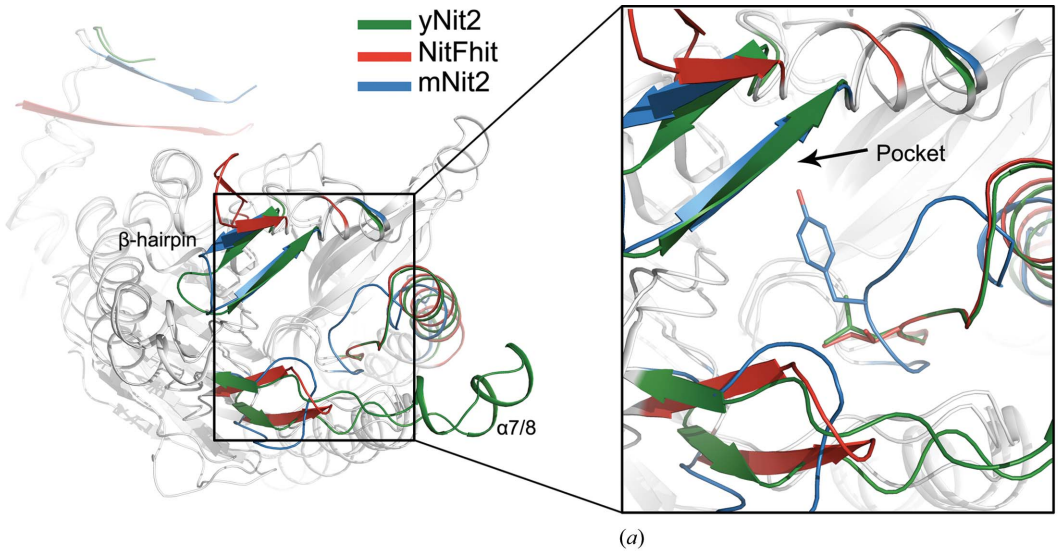


(*a*)

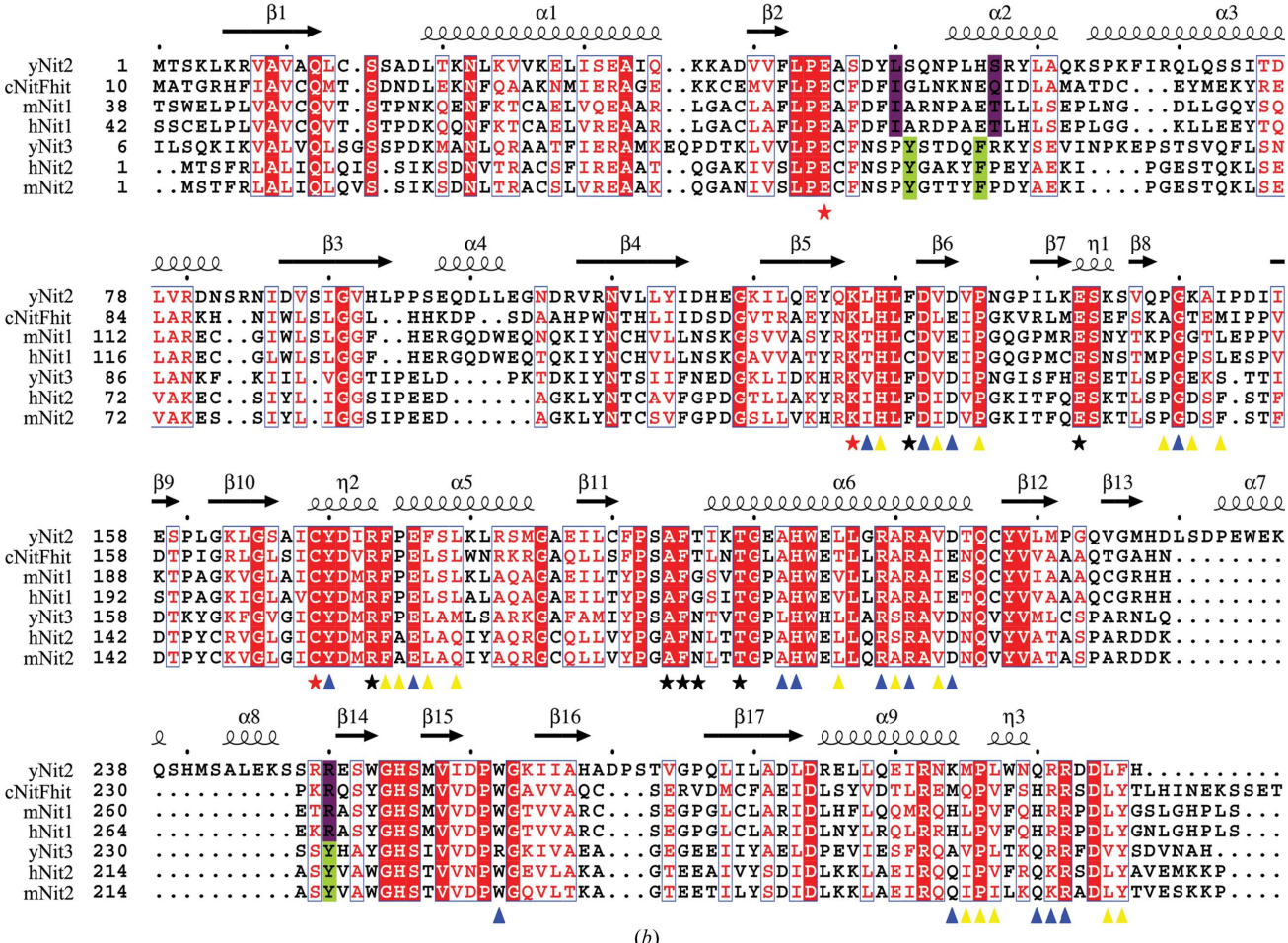


(*b*)

**Figure 2**
Comparison of yNit2 with its homologues. (*a*) Structural alignment of WT yNit2 with mNit2 and with the Nit region of cNitFhit. Noticeable structural differences among the three proteins are depicted. In the right panel, a loop of yNit2 (green) in the active-site region is similar in orientation to that of cNitFhit (red) but differs substantially from that of mNit2 (blue). As a result, the binding pocket is noticeably smaller in mNit2 relative to that of yNit2. (*b*) Sequence alignment of yNit2 with other Nit proteins from selected organisms. The amino-acid sequence of yNit2 is placed at the top. All other sequences are aligned below this sequence to show the best alignments of conserved residues. The alignment was performed by the method described in §2. Dots represent gaps. Secondary-structural elements of yNit2 are displayed above the sequences. Residues involved in dimer interactions are marked by blue (hydrogen bonds or salt bridges) and yellow (hydrophobic interactions) triangles below the sequences. Red and black stars below the sequences indicate the canonical catalytic triad residues and those involved in enzyme–ligand recognition, respectively. Purple and green highlighted residues in the sequence panels show unconserved residues surrounding the active site, which may cause differences in substrate specificity between yNit2 (or mammalian Nit1) and mammalian Nit2. These sequences were downloaded from UniProt as entries P47016 (yNit2), Q8VDK1 (mNit1), Q86X76 (hNit1), P49954 (yNit3), Q9NQR4 (hNit2), Q9JHW2 (mNit2) and O76463 (cNitFhit).

### 2.4. Structure analysis and figure preparation

The subunit composition of yNit2 was obtained by gel-filtration chromatography on a Superdex 200 10/300 GL column (GE Healthcare) and comparison of the $R_f$ of yNit2 with the $R_f$ values obtained for protein standards of precisely known molecular weights. In addition, the protein–protein interaction analysis and surface area of the dimer interface were calculated using the *PISA* (Krissinel & Henrick, 2007) module of the *CCP*4 software package. Hydrophobic interactions were analyzed using the *DIMPLOT* module of *LigPlot+* (Laskowski & Swindells, 2011), a GUI-based version of the *LIGPLOT* program (Wallace *et al.*, 1995). The substrate cavities were analyzed using *CAVER* (Chovancova *et al.*, 2012) at a neighbourhood range of 4.0 Å. The alignment was calculated by means of the *Clustal Omega* package (Sievers *et al.*, 2011) and drawn using *ESPript* (Gouet *et al.*, 2003). All figures showing crystal structures were prepared employing the *PyMOL* program (Schrödinger).

### 2.5. Enzymatic assay

yNit2 was expressed either as an N-$His_6$-tagged protein, which was used in crystallization studies, or as a C-$His_6$-tagged protein. All proteins used in enzymatic assays were produced by the procedures outlined above except that during the purification procedure all buffers contained 5 m*M* dithiothreitol (DTT). $\alpha$-KGM was produced essentially according to a previously described method (Krasnikov, Nostramo *et al.*, 2009). To assay the $\omega$-amidase activity of yNit2, we employed a coupled enzyme method first described by Hersh (1971) and later used by Jaisson *et al.* (2009). The 200 µl reaction mixture consisted of 100 m*M* Tris–HCl pH 8.5, 10 m*M* $NH_4Cl$, 5 m*M* DTT, 300 µ*M* NADPH, 22.7 m*M* $\alpha$-KGM, 2 U yeast glutamate dehydrogenase and 1 µg hNit2 or 10 µg yNit2 protein (WT or mutant). The rate of disappearance of NADPH ($\varepsilon_{340\ nm}$ = $6.23 \times 10^3\ M^{-1}\ l^{-1}$) as the product of $\alpha$-KGM hydrolysis (*i.e.* $\alpha$-KG) is reductively aminated to L-glutamate was continuously monitored at 303 K. All proteins used in the enzymatic assays were highly purified and exhibited a single band when subjected to SDS–PAGE (Supplementary Fig. S1[1]).

### 2.6. Mutagenesis

A C169S mutant was obtained from a pET28a construct of WT full-length yNit2 by site-directed mutagenesis using the mutagenic primers TTGGGCAGTGCCATTTCTTATGATATTCGCTTT and AAAGCGAATATCATAAGAAATGGCACTGCCCAA. An R250Y mutant (yNit2-R250Y) was produced in the same way as the C169S mutant with the mutagenic primers TCCAGGTATGAATCTTGGGGACACTCAATGGTCAT and AGATTCATACCTGGAGCTTTTTTCGAGAGCGCTCA. The mutations were confirmed by DNA sequencing. Curiously, yNit2-C169S contained a ligand in the active site when expressed and purified using the same procedures as used for WT yNit2. An OMIT map of this ligand was calculated using the *AutoBuild* module of *PHENIX* (Terwilliger *et al.*, 2008). Although not yet fully characterized, this ligand appears to be peptide-like and similar in shape to glutathione (GSH).

### 2.7. PDB accession codes

The atomic coordinates and structure factors of WT yNit2 have been deposited in the Protein Data Bank with accession code 4h5u. The accession codes for yNit2–$\alpha$-KG, yNit2–OA and yNit2-C169S complexed with a peptide-like ligand are 4hg3, 4hg5 and 4hgd, respectively.

## 3. Results

### 3.1. The overall structure of WT yNit2 is similar to those of other Nit proteins

In order to gain insight into the architectural basis and the mechanism by which yNit2 recognizes and binds substrates and ligands, in our first series of experiments recombinant WT yNit2 was crystallized and its X-ray structure was determined to 1.9 Å resolution and refined. The crystal parameters and refinement statistics are detailed in Table 1. Previous researchers have reported that rat liver Nit2/$\omega$-amidase is sensitive to air oxidation, presumably as a result of oxidation of the active-site cysteine (Hersh, 1971; Cooper *et al.*, 1985; Krasnikov, Chien *et al.*, 2009). Our data indicate that the active-site cysteine of yNit2 is also sensitive to oxidation. Thus, we found that Cys169 of yNit2 is oxidized to cysteinyl cacodylate in the crystallization buffer (Supplementary Fig. S2*a*). In our next series of experiments we determined the X-ray crystal structure of yNit2–$\alpha$-KG to 1.9 Å resolution. A similar determination was also made for yNit2–OA. It should be noted that all three of the crystallographic structures exhibit closely similar architectures, with an overall root-mean-square deviation (r.m.s.d.) of below 0.2 Å over the main-chain $C^\alpha$ atoms. Each asymmetric unit of yNit2 consists of two dimers along the noncrystallographic symmetry axis (Fig. 1*a*). All of the monomers of WT yNit2, yNit2–$\alpha$-KG and yNit2–OA are almost identical, with an r.m.s.d. of below 0.2 Å over 252 $C^\alpha$ atoms, except for a sequence from His228 to Glu251, which is assigned to an additional region ($\alpha$7-loop-$\alpha$8) that has obvious differences in conformation (r.m.s.d. of 0.1–2.6 Å; Supplementary Fig. S2*b*). The low dissociation barrier of this region (0.1 kcal $mol^{-1}$, calculated using the *PISA* program; 1 cal = 4.184 J) compared with the strong attraction between two monomers in the functional WT protein (30.2 kcal $mol^{-1}$, also calculated using *PISA*) suggests that the additional region may oscillate to regulate the volume of the active-site cavity during the catalytic cycle. In addition, a conserved $\beta$-hairpin from Asp132 to Lys142, $\beta$6-loop-$\beta$7, has a significantly high *B* factor, suggesting that this region is flexible.

As previously reported for the Nit domain of cNitFhit and for mNit2 (Pace & Brenner, 2001; Barglow *et al.*, 2008; Fig. 2*a*), yNit2 is an $\alpha$–$\beta$–$\beta$–$\alpha$ sandwich protein with a central pair of $\beta$-sheets that exclude waters, consisting of nine $\alpha$-helices

[1] Supplementary material has been deposited in the IUCr electronic archive (Reference: LV5038). Services for accessing this material are described at the back of the journal.

designated $\alpha$1–$\alpha$9, 17 $\beta$-strands designated $\beta$1–$\beta$17 and three $3_{10}$-helices designated $\eta$1–$\eta$3 (Fig. 2*b*). The $\beta$6/7 hairpin is positioned to cover the substrate tunnel above the ligand/substrate-binding site, while the flexible $\alpha$7/8 helix in combination with the $\beta$13/14 strand flanks the tunnel (Fig. 1*c*). In addition, the catalytic site of yNit2 closely resembles that of the Nit domain of cNitFhit and that of mNit2, with distances of 3.3 Å between the S atom of Cys169 and the carboxyl O atom of Glu45 and of 4.7 Å between the S atom of Cys169 and the $N^{\varepsilon}$ atom of Lys127 completing the canonical active-site catalytic triad.

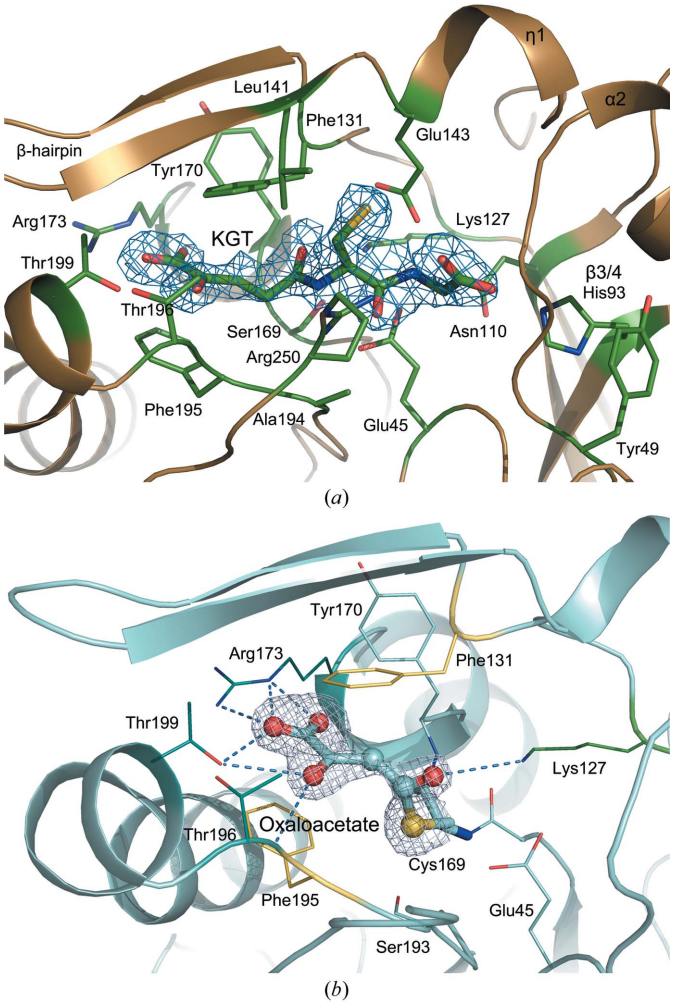


**Figure 3**
Active-site binding of a peptide-like ligand to yNit2-C169S and of OA to WT yNit. (*a*) Representation of the active site of yNit2-C169S . The mesh depicts the outline of a ligand that is present in the active site of the crystallized Nit2 mutant. This outline was obtained from an OMIT density map at 1.0$\sigma$ constructed around the ligand at a radius of 1.6 Å and indicates that the ligand may be GSH, a keto derivative or a similar molecule (see §4). The ligand is represented by a stick model within the mesh and is drawn as the open-chain form of the $\alpha$-keto analogue of GSH (*i.e.* KGT). Assuming that KGT is the actual ligand, more residues can theoretically participate in interactions with this ligand, such as His93/Asn110 of $\beta$3/4 and Arg250, than with the $\alpha$-KG and OA thioester intermediates. (*b*) OA bound covalently as a thioester to Cys169 in yNit2. The OA thioester is buried in the deep cavity below the $\beta$6/7 hairpin in a similar fashion to that noted for the $\alpha$-KG thioester (Fig. 1*b*). A $2F_o - F_c$ electron-density map at 1.0$\sigma$ is constructed around the ligand at a radius of 1.6 Å. Dashed lines represent hydrogen bonds and salt bridges. Protein–ligand interactions are similar to those noted for the $\alpha$-KG thioester intermediate in the active site of yNit2.

As noted in §1, mammalian Nit1 is a tumour suppressor, but the substrate specificity of this presumed amidase is unknown. Interestingly, however, mutation of the cysteine in the putative active site to an alanine does not affect the tumour-suppressor properties of Nit1, suggesting that Nit1 may have separate domains for catalysis and antitumour activity (Semba *et al.*, 2006). In the present work, we have likewise constructed an active-site mutant of yNit2. yNit2-C169S was crystallized and its X-ray structure was determined to 2.0 Å resolution with well refined parameters (Table 1). Surprisingly, we found a ligand binding to the active-site cavity of the mutated protein (Fig. 3*a*), despite the fact that the overall structure of the C169S mutant is very similar to those of WT yNit2, yNit–$\alpha$-KG and yNit2–OA. The density-contour map suggests that the ligand has a similar shape to that of GSH. A possible explanation is that the ligand is a natural substrate (or modulator). The inability to detect this compound in the WT enzyme may be due to hydrolysis by yNit2 before crystallization of WT yNit2, yNit2–$\alpha$-KG and yNit2–OA. The presumably inactive yNit2-C169S mutant may retain the natural substrate (or modulator) in its active site.

### 3.2. A thioester bond is formed between $\alpha$-KG (or OA) and Cys169

Although previous researchers (Hersh, 1972; Pace & Brenner, 2001; Krasnikov, Nostramo *et al.*, 2009) have suggested that the highly conserved catalytic cysteine residue of Nit2 and the putative catalytic cysteine of Nit1 may form an acyl-enzyme intermediate during catalytic deamidation of the substrate, no supporting X-ray crystallographic data were hitherto available. Moreover, it was not known how the enzyme recognizes its substrate(s). We have now obtained the X-ray crystal structure of a Nit protein containing an acyl (thioester) intermediate in the active site for the first time. Our X-ray crystal structure of yNit2–$\alpha$-KG clearly shows the presence of a thioester formed between the $\gamma$-carboxyl of $\alpha$-KG and the –SH moiety of the active-site cysteine, which has previously been speculated to be the intermediate in the catalytic hydrolysis of $\alpha$-KGM (Fig. 1*b*). Thr199 of $\alpha$6 and Arg173 of helix $\eta$2 immobilize the $\alpha$-carboxyl *via* a hydrogen bond and three salt bridges. This Thr199 also cooperates with Thr196 to form two hydrogen bonds to the $\alpha$-keto O atom of the thioester intermediate. The nearly parallel and highly aromatic rings of Phe131 and Phe195 'sandwich' the thioester intermediate and maintain a hydrophobic environment around the active site of the enzyme by hydrophobic interaction with neighbouring residues such as Val133, Leu141, Tyr170 and Trp204. In addition, the $\varepsilon$-$NH_2$ group of Lys127, between $\beta$5 and $\beta$6, forms a hydrogen bond to the carbonyl O atom of the thioester [—C(O)S—] portion of the intermediate; this $\varepsilon$-$NH_2$ group also hydrogen bonds to the highly conserved Glu45. A water molecule is interposed between the [—C(O)S—] moiety and Glu45. Another water molecule

abuts the S atom of Cys169 at a distance of 3.5 Å. In summary, these interactions help to bind functional groups of the enzyme–substrate intermediate prior to product (*i.e.* α-KG) release. The crystal structure of yNit2–OA shows that the α-carboxyl of OA also makes a thioester linkage to Cys169 (Fig. 3*b*). As in yNit2–α-KG, Phe131 and Phe195 also 'sandwich' the carbon skeleton of the thioester intermediate in yNit2–OA. Although the geometry about the active site is similar in yNit2–α-KG (and yNit2–OA) to that in WT yNit2, the cysteinyl cacodylate in the catalytic site is a confounding problem because it can form catalytically irrelevant interactions with water and other structures in the active site (Supplementary Fig. S2*a*). This consideration is one reason why we investigated the C169S mutant. The –OH group of the serine residue is much less likely to form a covalent adduct with the cacodylate ion in the crystallization buffer than is the active-site cysteine residue of WT yNit2. As indicated above, analysis of the yNit2-C169S mutant led to the discovery of an endogenous GSH-like ligand. The ligand bound at the active site of the C169S mutant appears to interact at more sites than do the thioester intermediates of yNit2–α-KG and yNit2–OA (Fig. 3*a*). For example, the GSH-like ligand may interact with residues such as His93, Asn110 and Arg250, which are conserved in various mammalian Nit1 proteins. The nature of the ligand and whether it binds in a similar fashion to that shown previously for the binding of dipeptide-α-CA probes to various Nit proteins (Barglow *et al.*, 2008) is currently under investigation.

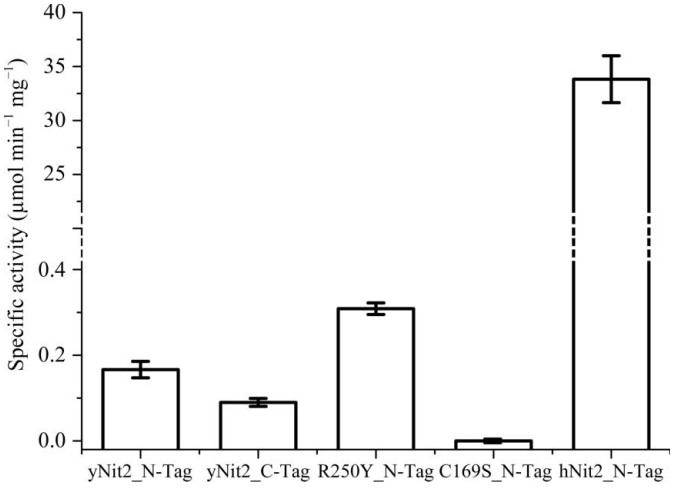


**Figure 4**
Specific activities of various Nit2 constructs. The relative specific activities were determined with α-KGM as a substrate at a concentration of 22.7 m*M*. This concentration of α-KGM is saturating for rat, mouse and human Nit2/ω-amidase (Krasnikov, Nostramo *et al.*, 2009; Jaisson *et al.*, 2009; Chien *et al.*, 2012). yNit2_N-tag is a yNit2 fusion protein containing an N-terminal $His_6$ tag (used in the crystallographic studies reported here). yNit2_C-Tag is a yNit2 fusion protein containing a C-terminal $His_6$ tag (a control to ensure that the low activity of the yNit2 used in the present study is not due to the $His_6$ tag at the N-terminus blocking the active site). R250Y_N-Tag is a yNit2 fusion protein containing an N-terminal $His_6$ tag and an R250Y mutation. C169S_N-Tag is a yNit2 fusion protein containing an N-terminal $His_6$ tag and a C169S mutation. hNit2_N-Tag is human Nit2, which was used as a control to show that a $His_6$ tag at the N-terminus does not disrupt the activity of the human homologue with α-KGM as substrate and as a positive control for an enzymatically active protein. The specific activity of yNit2 is extremely low (below 0.5% of that exhibited by hNit2) but is readily detectable. The specific activity with R250Y is slightly but significantly higher than that of WT yNit2. All assays were carried out in triplicate at 303 K; the error bar shows the standard deviation.

### 3.3. yNit2 has relatively low activity towards α-KGM

Inasmuch as (i) α-KG readily forms a thioester (the expected enzyme intermediate with α-KGM as substrate) at the active site of yNit2 (present work) and (ii) previous work has shown that α-KGM is an excellent substrate of mouse, human and rat Nit2 (Jaisson *et al.*, 2009; Krasnikov, Chien *et al.*, 2009; Krasnikov, Nostramo *et al.*, 2009; Chien *et al.*, 2012), we initially expected α-KGM to also be a good substrate of yNit2. However, the activity towards α-KGM was surprisingly low (Fig. 4). The specific activity of WT yNit2 was 0.17 ± 0.02 μmol min$^{-1}$ mg$^{-1}$ at 303 K (Fig. 4). As expected, the C169S mutant exhibited no discernible activity. To ensure that the low activity with yNit2 was not related to the assay conditions, the specific activity of $His_6$-tagged hNit2 was determined under identical assay conditions to those used for measurement of the specific activity of yNit2 (with α-KGM as substrate). The specific activity of hNit2 with α-KGM as substrate was found to be high (33.8 ± 2.2 μmol min$^{-1}$ mg$^{-1}$ at 303 K; Fig. 4). This value compares favourably with the specific activities reported previously for rat, mouse and human Nit2/ω-amidases with KGM as substrate (Hersh, 1971; Jaisson *et al.*, 2009; Krasnikov, Chien *et al.*, 2009; Chien *et al.*, 2012). The high specific activity of N-$His_6$-tagged hNit2 suggests that the low activity of WT yNit2 towards α-KGM does not arise from the N-$His_6$ tag in yNit2 interfering with the active site. Furthermore, in another control experiment it was

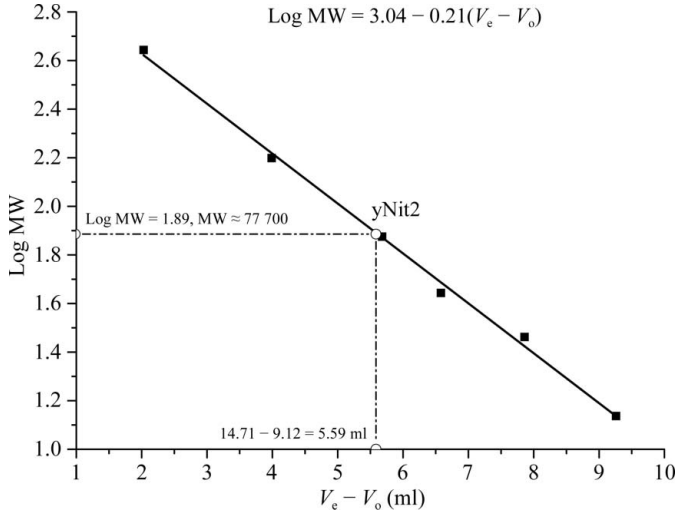


**Figure 5**
Gel filtration of yNit2 indicates that it is a dimer in solution. The dashed lines indicate the elution position of yNit2 on a Superdex 200 column relative to the elution positions of proteins of known molecular weight (filled squares) (*x* axis) and the log of the molecular weight (*y* axis). The calculated molecular weight of yNit2 is approximately 77 700, which indicates that the purified yNit2 is a dimer in solution.

shown that C-His$_6$-tagged yNit2 also has low activity with $\alpha$-KGM as substrate (0.09 $\pm$ 0.01 µmol min$^{-1}$ mg$^{-1}$ at 303 K).

### 3.4. yNit2 is a stable dimer in solution

Gel-filtration chromatography indicates that recombinant yNit2 forms a stable dimer in solution (Fig. 5 and Supplementary Fig. S3). The calculated molecular weight of the recombinant yNit2 monomer is 38 235 and its apparent molecular weight calculated from the elution volume of the gel filtration is about 77 700. These results suggest that yNit2 is in the form of a dimer in solution. In addition, the crystal structure of yNit2 shows that the $\beta$6, $\alpha$5 and $\alpha$6 segments of the two subunits along a pseudo-crystallographic twofold symmetric axis are combined to form a major interface that holds the two subunits together (Fig. 1*a*). Moreover, the C-termini of the two subunits align along the axis with the aid of 14 hydrogen bonds and eight salt bridges. Hydrophobic interactions involved in the dimer interface also enhance the stability of the dimer. All these interactions form an extensive interface area of 1942 Å$^2$, encompassing about 14% of the total surface area of each monomer. This considerable juxtapositioning of monomer surfaces results in the formation of a very stable dimer. All of the residues involved in the subunit interactions are highly conserved among the seven selected examples in the Nit family shown in Fig. 2(*b*) except for a few residues involved in main-chain hydrogen-bond interactions or hydrophobic interactions, which are less conserved. Remarkably, Asp134 and Asp132 of the $\beta$6/7 hairpin interact with the C-terminal residues Lys294 and Gln300, respectively, of the other monomer through hydrogen bonding. Tyr170, a residue close to the catalytic Cys169 in one monomer, is also locked to Gln300 of the other monomer through a 2.7 Å hydrogen bond. Thus, this Gln300 mediates the interaction between Tyr170 of the catalytic site and Asp132 of the $\beta$6/7 hairpin (Fig. 1*a*). The importance of this interaction is discussed below.

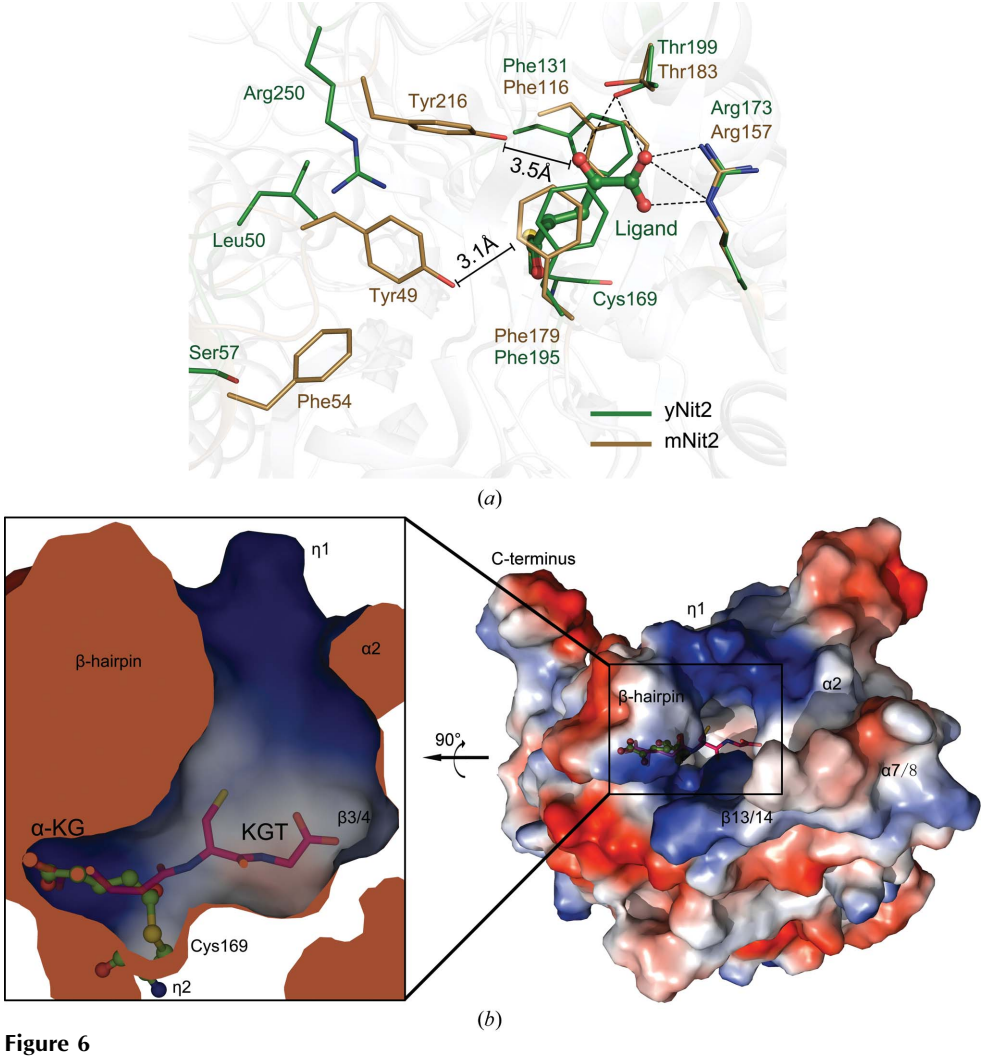


**Figure 6**
Cavity features of Nit2. (*a*) Superimposition of the $\alpha$-KG intermediate in the active site of yNit2–$\alpha$-KG with that of mNit2. Tyr49 and Tyr216 of mNit2 are proposed to bind to $\alpha$-KGM. No residues comparable to Tyr49 and Tyr216 in mNit2 are present in the active site of yNit2. Note also that when viewed from above these tyrosine residues show that the volume of the active site is smaller in mNit2 than in yNit2. (*b*) Cross-sectional view (left panel) and top view (right panel) of the active site of yNit2–$\alpha$-KG. The cavity encompassing the boot-like active site is shown in electrostatic potential surface mode. $\alpha$-KG is shown as a thioester intermediate with Cys169 (ball-and-stick representation) pointing to the 'toe' of the active site. Superimposed is a stick representation of the peptide (GSH-like) ligand that is noted to be present in the active site of the crystallized yNit2-C169S mutant. In this depiction, the GSH-like structure is assumed to be KGT. The right panel depicts the surface electrostatics of one subunit arranged so that the 'mouth' of the active site is in the centre of the field of view. A stick representation of KGT is shown in this cavity, part of which overlaps with the $\alpha$-KG thioester intermediate. Note that a $\beta$-hairpin overlies part of the active site so that a portion of the KGT is actually below this lid. Positively charged, negatively charged and neutral residues in the subunit surface are shown in blue, red and white, respectively.

## 4. Discussion

### 4.1. Importance of the yNit2 dimer in the putative catalytic process

We have found that $\alpha$-KG reacts with WT yNit2 to form a thioester intermediate at the active site that is the predicted reaction intermediate in mammalian Nit2/$\omega$-amidase-catalyzed hydrolysis of $\alpha$-KGM (the $\alpha$-keto analogue of glutamine). Similarly, we have found that OA reacts with WT yNit2 to form a thioester intermediate at the active site that is the predicted reaction

intermediate in the mammalian Nit2/$\omega$-amidase enzyme-catalyzed hydrolysis of $\alpha$-KSM (the $\alpha$-keto analogue of asparagine). We hypothesize that the formation of these enzyme thioester intermediates is facilitated by the structure of the dimer. Our reasoning is as follows. Tyr170, which is involved in the formation of the dimer interface, is close to the catalytically indispensable Cys169 and is also in close proximity to Arg173 of the $\eta$2 helix (Fig. 1*b*). Our analysis further suggests that Gln300 mediates the interaction between the $\beta$6/7 hairpin and the catalytic site, thereby providing another link between dimerization and the catalytic process. We suggest that due to the close proximity of the active site to the dimer interface of yNit2, the dimer is poised to sense conformational changes at the active site, which in turn influences the structure of the $\beta$6/7 hairpin lid, triggering the enzymatic reaction. The closing of the lid may precede the formation of the thioester intermediate by conformational changes in the Lys127 and Phe131 residues, which are positioned alongside the hairpin lid. We further suggest that a water molecule confined by Glu45 attacks the Cys169 thioester intermediate, resulting in release of the product $\alpha$-KG (or OA).

### 4.2. The substrate specificity of yNit2

The residues of yNit2 that interact with the $\alpha$-KG thioester are highly conserved in Nit proteins (Fig. 2*b*). As noted above, previous studies have shown that glutamine is not a substrate of partially purified rat liver $\omega$-amidase (Meister, 1954; Meister *et al.*, 1955) or highly purified hNit2/$\omega$-amidase (Chien *et al.*, 2012). In our experiments, it is also not a substrate of yNit2 (data not shown). Our study of yNit2–$\alpha$-KG and yNit2–OA suggests that the $\alpha$-KG/OA thioester ligand forms a $\pi$,$\pi$-enhanced anion–$\pi$ interaction with the $\pi$ system of Phe195, while Phe131 of the lid maintains the hydrophobic environment in the vicinity of the ligand carbon skeleton. The $\pi$,$\pi$-enhanced anion–$\pi$ interaction is an example of the recently reported anion–$\pi$ interaction (Dawson *et al.*, 2010), with a $\pi$,$\pi$-conjugated anion located at the anion site. This kind of interaction involving an anion and an aromatic ring (termed an $\eta$6-type anion–$\pi$ interaction), although rarer than the well established cation–$\pi$ interactions, has now been detected in several protein tertiary structures and in DNA–protein interactions (Chakravarty *et al.*, 2012). Based on the considerations discussed by Chakravarty and coworkers, we suggest that the anionic $\alpha$-carboxylate functional groups of the substrates $\alpha$-KGM and $\alpha$-KSM conjugate with the adjacent $\alpha$-keto group to form a y-shaped $\pi$ system with a negative charge. This $\pi$ system interacts with another $\pi$ system of the benzene ring of Phe195. Glutamine does not possess an $\alpha$-keto-acid group and therefore cannot generate the above-described $\pi$ system. It is possible that yNit2 recognizes the $\alpha$-keto group but not the $\alpha$-amino group using this kind of interaction. We also note that mNit2 has a phenylalanine in the active site (Fig. 6*a*). We suggest that the $\pi$,$\pi$-enhanced anion–$\pi$ interaction with the $\pi$ system of a conserved active-site phenylalanine may be a common mechanism for Nit proteins to recognize the $\alpha$-keto group of substrates.

As noted in §1, highly purified recombinant mNit1 has a very low activity towards $\alpha$-KGM. In the present work, we show that yNit2 also has low, but detectable, activity towards $\alpha$-KGM compared with mammalian Nit2/$\omega$-amidase proteins. Thus, it is highly likely that the active sites of yNit2 and mNit1 have some features in common. In this regard, Arg250 of yNit2 is replaced by a tyrosine residue in mammalian Nit2 proteins (Tyr216 in mNit2) but is conserved in mammalian Nit1 (Fig. 2*b*). Our analysis shows that Tyr216 of mNit2 can hydrogen bond to the $\alpha$-keto O atom of the $\alpha$-KG thioester intermediate in the active site. However, in the case of yNit2 Arg250 cannot form such a hydrogen bond (Fig. 6*a*). It is interesting to note that the specific activity at 303 K of the R250Y mutant of yNit2 (labelled R250Y_N-Tag in Fig. 4) of $0.31 \pm 0.01$ µmol min$^{-1}$ mg$^{-1}$ with $\alpha$-KGM as the substrate is significantly increased relative to that of WT yNit2 (labelled yNit2_N-Tag in Fig. 4) of $0.17 \pm 0.02$ µmol min$^{-1}$ mg$^{-1}$ ($p < 0.01$). yNit2-R250Y exhibits a relative specific activity of 0.9% compared with that of hNit2 with $\alpha$-KGM as the substrate (Fig. 4). Overall, our analysis indicates that the tyrosine residue enhances the interaction between the enzyme and the substrate in the complex to stabilize sandwich formation in mammalian Nit2. Furthermore, Tyr49 of mNit2, a residue that interacts with Lys112 and Glu128 (corresponding to Lys127 and Glu143 of yNit2) may be near the [$-$C(O)S$-$] moiety of the $\alpha$-KG thioester (Fig. 6*a*). Cooperating with Lys112, Tyr49 may hydrogen bond to the $\gamma$-amide moiety of $\alpha$-KGM in a manner suitable for nucleophilic attack by the cysteine residue in the active site or for promoting the release of the ammonia product. In addition, the peptide region from residues 48–66 of yNit2 is structurally different from that of residues 46–64 of mNit2 (Figs. 2*a* and 2*b*). Attempts to change the amino-acid sequence 48–66 of yNit2 to match the amino-acid sequence 46–64 of hNit2 were unsuccessful due to inclusion-body formation during protein expression (data not shown). We suggest that the conformation of this region is more restricted in mammalian Nit2 proteins, allowing binding and efficient hydrolysis of $\alpha$-KSM or $\alpha$-KGM and various $\gamma$-esters of $\alpha$-KG, but not of larger molecules. On the other hand, the conformation of this region may allow the binding of much larger substrates to yNit2 (and perhaps also to mammalian Nit1 proteins) than is possible in mammalian Nit2/$\omega$-amidase proteins (Fig. 6*b*). If this reasoning is correct, then $\alpha$-KGM may be a relatively poor substrate of yNit2 because it can only occupy a portion of the available space in the active site. Thus, in terms of substrate specificity yNit2 may be a closer homologue of mammalian Nit1 than it is of mammalian Nit2.

Our findings indicate that whatever the structures of natural substrates of yNit2 are, $\alpha$-KG (or OA) with a thioester linkage to the active-site cysteine is almost certainly an enzyme intermediate. $\alpha$-KGM fulfils this criterion, but as noted above it is a relatively poor substrate. The finding of a ligand in the active site of the yNit2-C169S mutant is interesting. This ligand, which is considerably larger than $\alpha$-KGM, is sufficiently large to bind to the relatively spacious active site of yNit2. Although attempts to identify this ligand by mass spectrometry were unsuccessful, the requirement for an $\alpha$-KG

thioester intermediate and the finding of a molecule roughly the shape of GSH in the active site of the mutant protein suggests that yNit2 may catalyze the hydrolysis of N-substituted analogues of α-KGM in which the substituent on the amide N atom is relatively large. One possibility is that the substrate is α-KG in which the γ-carboxyl has an amide (γ-peptide) linkage to an amino acid or dipeptide. Another possibility is α-KSM in which the β-carboxyl has an amide linkage to an amino acid or dipeptide. We have tentatively identified the ligand at the active site of yNit2-C169S as GSH-like. This is a reasonable assumption based on cavity analysis (Fig. 6*b*) and the fact that GSH is present in *E. coli* (in which yNit2-C169S was overexpressed), in which it plays a crucial role in detoxification processes (Allocati *et al.*, 2009). A tentative structure of the GSH-like molecule in the active site of yNit2-C169S, which can be used as a framework for future studies, is the α-keto analogue of GSH, namely KGT (Supplementary Fig. S4). In this regard, it is interesting to note that Otani & Meister (1957) showed that glutathione, L-γ-glutamylglycine, L-γ-glutamyl-L-alanine and L-γ-glutamyl-β-alanine are substrates of snake-venom L-amino-acid oxidase. Presumably, the initial product in each case will be an N-substituted α-KGM. However, before these amide-substituted analogues of α-KGM can be considered as potential substrates of yNit2 a caveat must be discussed. α-KGM overwhelmingly exists as a lactam (2-hydroxy-5-oxoproline) in solution. Under physiological conditions only 0.3% is in the open-chain form, which is the substrate for mammalian Nit2/ω-amidase (Hersh, 1971). The rate of interconversion between the lactam and open-chain forms is specific base ($OH^-$) catalyzed. At pH values of above 8.0 the rate of interconversion is sufficiently rapid so as not to be rate-limiting for the amounts of ω-amidase that are usually assayed (Hersh, 1971). Hence, ω-amidase assays with α-KGM as substrate are usually performed at pH values of ∼8–8.5. Typical α-keto acids are readily decarboxylated by ceric sulfate. However, Otani & Meister (1957) were unable to detect any decarboxylation of γ-(α-ketoglutaryl)glycine, γ-(α-ketoglutaryl)-β-alanine or γ-(α-ketoglutaryl)-L-alanine in the presence of ceric sulfate and suggested that these α-keto acids are in a cyclized (lactam) form. The α-keto-acid analogue of GSH was not tested but is also expected to be in a lactam form. There are several possibilities that might allow amidase activity with these γ-ketoglutaryl derivatives despite the equilibrium favouring the lactam form: (i) as for α-KGM there is a small amount of the open-chain form in equilibrium with the lactam of the γ-(α-ketoglutaryl) peptide, (ii) the lactam form is the substrate or (iii) the enzyme binds the lactam form but interactions within the active site favour opening of the ring. Otani & Meister (1957) also showed that β-L-aspartylglycine and β-L-aspartyl-L-alanine are substrates of L-amino-acid oxidase. In this case, the α-keto acids generated by the action of L-amino-acid oxidase on these peptides (*i.e.* β-oxalacetylglycine and β-oxalacetyl-L-alanine, respectively) were shown to be in the open-chain configuration. Otani & Meister (1957) further showed that β-oxalacetylglycine and β-oxalacetyl-L-alanine participate in transamination reactions with glutamine in the presence of rat liver extracts. Transamination of γ-glutamyl peptides and β-aspartyl peptides was not investigated by these authors, but since transamination reactions are usually reversible it is highly plausible that β-aspartyl peptides (and γ-glutamyl peptides) are potential transaminase substrates *in vivo*. If this is the case then yNit2 (and possibly mammalian Nit1) may be involved in recycling α-KG and OA following nonspecific transamination of γ-glutamyl and β-aspartyl peptides. In other words, yNit2 may be a salvage or repair enzyme whose biological role is to counteract the possible deleterious effects of nonspecific transamination of γ-glutamyl (or β-aspartyl) peptides.

### 4.3. Does Nit2 participate in glutamine metabolism in yeast?

A glutamine transaminase-ω-amidase pathway has been well documented to occur in the yeast *S. cerevisiae* (Soberón & González, 1987). Thus, despite the fact that the specific activity of purified yNit2 with α-KGM as a substrate is relatively low compared with that exhibited by mammalian Nit2/ω-amidase enzymes, the activity towards α-KGM may be sufficient to meet the nutritional needs of the organism. On the other hand, it is also possible that yNit2 (unlike mammalian Nit2/ω-amidase proteins) may be under allosteric regulation by an unknown factor in response to changes in nitrogen metabolism. Finally, it is also possible that a different enzyme to that employed by mammals subsumes the role of hydrolyzing α-KGM in yeast. One possibility is yeast Nit3 (yNit3), which has more conserved residues in its putative active site (residues highlighted in green in Fig. 2*b*) in comparison to mNit2 than does yNit2. These possibilities are currently under investigation.

## 5. Conclusion

The ligands that have been shown to bind in the catalytic cavity have revealed a common molecular-recognition mechanism for substrates and enzymes within the Nit protein family. It is now well established that mammalian Nit2/ω-amidase possesses strong binding regions in the active site for the α-carboxyl and α-keto moieties of its substrates (α-KGM and α-KSM; Chien *et al.*, 2012). Furthermore, the present findings strongly suggest that yNit2 and possibly yNit3 and mammalian Nit1 possess strong binding sites for the α-carboxyl and α-keto moieties of the natural substrates/products. Interestingly, our evidence suggests that the various Nit proteins interact with the α-keto moiety of their respective substrates *via* π,π-enhanced anion–π interactions, whereas these proteins interact with the functional carboxyl moiety of their respective substrates *via* hydrogen bonding and salt bridges. Moreover, our findings suggest that homodimerization may contribute to the catalytic properties of Nit proteins. On the other hand, there are also marked differences in active-site topology among the various Nit proteins. For example, although it is phylogenetically related to mammalian Nit2, yNit2 appears to have an active site that is remarkably distinct from that of mammalian Nit2, which may contribute to

the different substrate specificity of yNit2 compared with that of mammalian Nit2. In certain aspects, the active site of yNit2 more closely resembles the putative active site of mammalian Nit1 than it does the active site of mammalian Nit2, especially in regard to the size of the active-site cavity, which is much larger in yNit2 and mammalian Nit1 than in mammalian Nit2. It is also possible that this difference may relate to the differing mechanisms used by yeasts compared with mammals for maintaining nitrogen homeostasis. Particularly interesting is the finding of a bulky ligand in the active site of the crystallized yNit2-C169S mutant. As noted above, although this ligand originated from the *E. coli* cells overexpressing yNit2 it is probable that this ligand is also present naturally in yeast cells. This ligand may be the natural substrate of WT yNit2 or it may be a regulator of enzyme activity. Work is ongoing to identify this ligand. Identification of this ligand will not only further our understanding of the catalytic properties of yNit2, but will also shed light on the natural substrate(s) and metabolic roles of the mammalian tumour-suppressor protein Nit1.

We would like to thank the staff of SSRF for help in data collection and processing. This work was supported by grants from the Chinese Ministry of Science and Technology (grant Nos. 2012CB917200 and 2009CB825500) and the Chinese National Natural Science Foundation (grant Nos. 31130018 and 31170726).

## References


Adams, P. D. *et al.* (2010). *Acta Cryst.* D**66**, 213–221.

Allocati, N., Federici, L., Masulli, M. & Di Ilio, C. (2009). *FEBS J.* **276**, 58–75.

Barglow, K. T. & Cravatt, B. F. (2006). *Angew. Chem. Int. Ed.* **45**, 7408–7411.

Barglow, K. T., Saikatendu, K. S., Bracey, M. H., Huey, R., Morris, G. M., Olson, A. J., Stevens, R. C. & Cravatt, B. F. (2008). *Biochemistry*, **47**, 13514–13523.

Chakravarty, S., Sheng, Z.-Z., Iverson, B. & Moore, B. (2012). *FEBS Lett.* **586**, 4180–4185.

Chen, V. B., Arendall, W. B., Headd, J. J., Keedy, D. A., Immormino, R. M., Kapral, G. J., Murray, L. W., Richardson, J. S. & Richardson, D. C. (2010). *Acta Cryst.* D**66**, 12–21.

Chien, C.-H., Gao, Q.-Z., Cooper, A. J. L., Lyu, J.-H. & Sheu, S.-Y. (2012). *J. Biol. Chem.* **287**, 25715–25726.

Chovancova, E., Pavelka, A., Benes, P., Strnad, O., Brezovsky, J., Kozlikova, B., Gora, A., Sustr, V., Klvana, M., Medek, P., Biedermannova, L., Sochor, J. & Damborsky, J. (2012). *PLoS Comput. Biol.* **8**, e1002708.

Cooper, A. J. L., Duffy, T. E. & Meister, A. (1985). *Methods Enzymol.* **113**, 350–358.

Dawson, R. E., Hennig, A., Weimann, D. P., Emery, D., Ravikumar, V., Montenegro, J., Takeuchi, T., Gabutti, S., Mayor, M., Mareda, J., Schalley, C. A. & Matile, S. (2010). *Nature Chem.* **2**, 533–538.

Emsley, P., Lohkamp, B., Scott, W. G. & Cowtan, K. (2010). *Acta Cryst.* D**66**, 486–501.

Gouet, P., Robert, X. & Courcelle, E. (2003). *Nucleic Acids Res.* **31**, 3320–3323.

Hersh, L. B. (1971). *Biochemistry*, **10**, 2884–2891.

Hersh, L. B. (1972). *Biochemistry*, **11**, 2251–2256.

Howden, A. J. & Preston, G. M. (2009). *Microb. Biotechnol.* **2**, 441–451.

Huebner, K., Saldivar, J. C., Sun, J., Shibata, H. & Druck, T. (2011). *Adv. Enzyme Regul.* **51**, 208–217.

Jaisson, S., Veiga-da-Cunha, M. & Van Schaftingen, E. (2009). *Biochimie*, **91**, 1066–1071.

Krasnikov, B. F., Chien, C.-H., Nostramo, R., Pinto, J. T., Nieves, E., Callaway, M., Sun, J., Huebner, K. & Cooper, A. J. L. (2009). *Biochimie*, **91**, 1072–1080.

Krasnikov, B. F., Nostramo, R., Pinto, J. T. & Cooper, A. J. L. (2009). *Anal. Biochem.* **391**, 144–150.

Krissinel, E. & Henrick, K. (2007). *J. Mol. Biol.* **372**, 774–797.

Laskowski, R. A. & Swindells, M. B. (2011). *J. Chem. Inf. Model.* **51**, 2778–2786.

Lin, C.-H., Chung, M.-Y., Chen, W.-B. & Chien, C.-H. (2007). *FEBS J.* **274**, 2946–2956.

McCoy, A. J., Grosse-Kunstleve, R. W., Adams, P. D., Winn, M. D., Storoni, L. C. & Read, R. J. (2007). *J. Appl. Cryst.* **40**, 658–674.

Meister, A. (1953). *J. Biol. Chem.* **200**, 571–589.

Meister, A. (1954). *J. Biol. Chem.* **210**, 17–35.

Meister, A., Levintow, L., Greenfield, R. E. & Abendschein, P. A. (1955). *J. Biol. Chem.* **215**, 441–460.

Meister, A., Sober, H. A., Tice, S. V. & Fraser, P. E. (1952). *J. Biol. Chem.* **197**, 319–330.

Moriarty, N. W., Grosse-Kunstleve, R. W. & Adams, P. D. (2009). *Acta Cryst.* D**65**, 1074–1080.

Murshudov, G. N., Skubák, P., Lebedev, A. A., Pannu, N. S., Steiner, R. A., Nicholls, R. A., Winn, M. D., Long, F. & Vagin, A. A. (2011). *Acta Cryst.* D**67**, 355–367.

O'Reilly, C. & Turner, P. D. (2003). *J. Appl. Microbiol.* **95**, 1161–1174.

Otani, T. T. & Meister, A. (1957). *J. Biol. Chem.* **224**, 137–148.

Otwinowski, Z. & Minor, W. (1997). *Methods Enzymol.* **276**, 307–326.

Pace, H. C. & Brenner, C. (2001). *Genome Biol.* **2**, reviews0001.1–reviews0001.9.

Pace, H. C., Hodawadekar, S. C., Draganescu, A., Huang, J., Bieganowski, P., Pekarsky, Y., Croce, C. M. & Brenner, C. (2000). *Curr. Biol.* **10**, 907–917.

Saldivar, J. C., Bene, J., Hosseini, S. A., Miuma, S., Horton, S., Heerema, N. A. & Huebner, K. (2013). *Adv. Biol. Regul.* **53**, 77–85.

Semba, S., Han, S.-Y., Qin, H. R., McCorkell, K. A., Iliopoulos, D., Pekarsky, Y., Druck, T., Trapasso, F., Croce, C. M. & Huebner, K. (2006). *J. Biol. Chem.* **281**, 28244–28253.

Sievers, F., Wilm, A., Dineen, D., Gibson, T. J., Karplus, K., Li, W., Lopez, R., McWilliam, H., Remmert, M., Söding, J., Thompson, J. D. & Higgins, D. G. (2011). *Mol. Syst. Biol.* **7**, 539.

Soberón, M. & González, A. (1987). *J. Gen. Microbiol.* **133**, 9–14.

Sun, J., Liu, J., Pan, X., Quimby, D., Zanesi, N., Druck, T., Pfeifer, G. P., Croce, C. M., Fong, L. Y. & Huebner, K. (2011). *Carcinogenesis*, **32**, 351–358.

Sun, J., Okumura, H., Yearsley, M., Frankel, W., Fong, L. Y., Druck, T. & Huebner, K. (2009). *J. Cell. Biochem.* **107**, 1097–1106.

Terwilliger, T. C., Grosse-Kunstleve, R. W., Afonine, P. V., Moriarty, N. W., Zwart, P. H., Hung, L.-W., Read, R. J. & Adams, P. D. (2008). *Acta Cryst.* D**64**, 61–69.

Vagin, A. & Teplyakov, A. (2010). *Acta Cryst.* D**66**, 22–25.

Wallace, A. C., Laskowski, R. A. & Thornton, J. M. (1995). *Protein Eng.* **8**, 127–134.

Winn, M. D. *et al.* (2011). *Acta Cryst.* D**67**, 235–242.

Zhang, H., Hou, Y.-J., Han, S.-Y., Zhang, E.-C., Huebner, K. & Zhang, J. (2009). *Int. Immunol.* **21**, 691–703.